



## ORIGINAL ARTICLE

# Biomass-derived active carbon (AC) modified TiO<sub>2</sub> photocatalyst for efficient photocatalytic reduction of chromium (VI) under visible light



Mabkhoot Alsaiari

Promising Centre for Sensors and Electronic Devices (PCSED), Advanced Materials and Nano-Research Centre, Najran University, P.O. Box: 1988, Najran 11001, Saudi Arabia  
Empty Quarter Research Unit, Department of Chemistry, Faculty of Science and Arts at Sharurah, Najran University, Saudi Arabia

Received 3 April 2021; accepted 8 June 2021  
Available online 17 June 2021

## KEYWORDS

Biomass derived active carbon;  
TiO<sub>2</sub>;  
Sol-gel;  
Photocatalyst;  
Photo-reduction of chromium (VI)

**Abstract** Creation of novel visible light efficient photocatalyst requires great effort and it is always a challenging task for scientific community. The present report demonstrates the designing of highly effective biomass derived active carbon (AC) modified TiO<sub>2</sub> photocatalyst and its utilization towards the photocatalytic reduction of chromium (VI) to chromium (III) in presence of citric acid under visible light. The photocatalyst comprising of various wt% of AC doped m-TiO<sub>2</sub> has been fabricated by straightforward sol-gel approach followed by a sonication technique. The fabricated photocatalysts composed of TiO<sub>2</sub> nanoparticles (particles size in the range of 8–20 nm) are entangled with biomass derived AC nanosheets. FTIR analysis further confirmed the successful creation of hetro-structures between AC and TiO<sub>2</sub>. All hybrid nanostructures showed lower band gap value i.e. in the visible absorption spectral region. The developed photocatalysts were found to be significantly boosted towards the photo-reduction of chromium (VI) to chromium (III) with a photo-reduction efficiency of 94.7% after 25 min of irradiation, compared to pure TiO<sub>2</sub> which gave a conversion rate of 72.10%. The enhanced photocatalytic reduction efficiencies were related to the effectual separation of charge carriers i.e. electron and holes pairs as confirmed by the photoluminescence (PL) analysis. Besides this, the presence of citric acid in dichromate solution enhances the transformation rate due to its involvement in oxidation reaction, which helps in retardation of unacceptable re-oxidation process of Cr (III) to Cr (VI). Furthermore, the newly designed photocatalyst showed excellent recyclability and reusability. Achieved results and involved reaction mechanism have been thoroughly addressed and elucidated.

© 2021 The Author. Published by Elsevier B.V. on behalf of King Saud University. This is an open access article under the CC BY license (<http://creativecommons.org/licenses/by/4.0/>).

E-mail address: [mabkhoot.alsaiari@gmail.com](mailto:mabkhoot.alsaiari@gmail.com)

Peer review under responsibility of King Saud University.



## 1. Introduction

Harmful and toxic substances like dyes, pesticides, industrial waste, and lab chemicals are directly introduced into

surrounding vicinity without or with minimal treatment. These notorious pollutants are extremely hazardous to human as well as marine life (Faisal et al., 2018). Former treatment procedures including for example adsorption, precipitation, flocculation and biological/chemical approaches are not efficient enough as they converted the noxious compounds from one form to other instead of complete elimination (Faisal et al., 2018). Therefore, the present scenario urgently requires a target-oriented treatment plan for the rectification of such pollutants. Recently promising outcomes of advanced oxidation processes attracted several research groups across the globe to explore the possibilities for the successful achievement of their goals (Bouزيد et al., 2015). Semiconductor oriented photocatalytic destruction of toxic moieties nowadays is a subject of great interest and found to be highly competent for the destruction/removal of a variety of toxic analytes (Faisal et al., 2021).

Titanium dioxide ( $\text{TiO}_2$ ) is a worldwide recognized as a proficient photocatalyst due its highly promising feature like high photocatalytic efficiency, sufficient chemical and biological stability, cost effective synthesis, non-noxious nature and long-term stability (Sanad et al., 2018; Faisal et al., 2018; Ismail et al., 2018).  $\text{TiO}_2$  mediated photocatalytic removal of hazardous environmental pollutants is a promising approach specifically towards the treatment of bio-recalcitrant organic waste product (Faisal et al., 2018; Sanad et al., 2018; Faisal et al., 2018; Ismail et al., 2018). Titania (like anatase  $\text{TiO}_2$ ) due to its outsized band gap (3.20 eV) limits to make use of just a slight segment of visible solar spectrum i.e. 4–5% (Fateh et al., 2011). Recently photocatalysts having perfect synchronization with visible light have attracted considerable attention. Therefore, in order to utilize clean energy competently, proper material selection is essentially required.

Designing of  $\text{TiO}_2$  with mesoporous framework is an effective approach for high photocatalytic performance, since well-organized mesoporous structure could offer seamless channeling to facilitate responsive intra-particle molecular transfer of the substrate molecules (Niu et al., 2018). Furthermore, highly crystalline framework of designed photocatalysts would enhance the transference of produced electron and hole pairs from bulk to the surface of the  $\text{TiO}_2$  particles, leading to suppression of recombination process and resulting in boosting the photonic efficiency of the material (Zhang et al., 2020; Petronella et al., 2019). Still, creation of semiconductor metal oxides possessing mesoporous framework and crystalline pore walls requires further effort (Petronella et al., 2019). Even though, mesoporous  $\text{TiO}_2$  has already been developed long back by Antonelli group in 1995 (Antonelli and Ying, 1995), still further work is necessary for the creation of well-organized mesoporous  $\text{TiO}_2$  framework with crystalline walls (Muniandy et al., 2017; Shayegan et al., 2018).

In recent years, concrete efforts have been put into action to improve the adsorption capability of  $\text{TiO}_2$  in visible region like decorating with precious metals (Mahmoud et al., 2012; Venkatachalam et al., 2007; Ismail et al., 2012), transition metals (Kang, 2003; Arpac et al., 2007; Ismail and Bahnemann, 2010), coupling with organic constituents (Sonawane et al., 2004; Yang et al., 2012) and to different nonmetal atoms (Nam et al., 2012; Charanpahari et al., 2012). Band gap narrowing of  $\text{TiO}_2$  by combining with non-metallic anions (N, C, S and F) was found to be quite effec-

tive than routine approaches towards the creation of efficient visible light driven photocatalysts. Utilization of nonmetal cations for improving the photocatalytic performance of  $\text{TiO}_2$  was well reported in literature (Ohno et al., 2004; Lv et al., 2012). Kangle group reported the synergistic effect of cysteine modified different nonmetal doped  $\text{TiO}_2$  hollow microspheres towards the photocatalytic activity and also conducted a relative investigation of N, C and Bi mixed with  $\text{TiO}_2$  nanostructures under UV and visible light illumination (Lv et al., 2009). Ohno et al. testified that doping of S cation in  $\text{TiO}_2$  immensely enhanced the performance under visible light by improving the visible light adsorption skills of designed structure (Ohno et al., 2004).

It has been well documented that deliberate incorporation of carbon into  $\text{TiO}_2$  lattice is an efficient method towards the improvement of adsorption capabilities of designed photocatalyst (Kang et al., 2008; Hahn et al., 2009) and also to expand the operational range towards the visible region (Li et al., 2005; Ren et al., 2007). Integration of carbon can increase the conductivity of  $\text{TiO}_2$ , as it could smoothen the charge transfer from the bulk to the surface of  $\text{TiO}_2$  resulting in enhancement of oxidation reactions at the surface of  $\text{TiO}_2$  (Xiao and Ouyang, 2009). Sakthivel group successfully synthesized a carbon-modified titania framework by hydrolysis of titanium tetrachloride with tetrabutylammonium hydroxide with a calcination at 400 °C. The prepared nanostructures produced superior photocatalytic activity by degrading 4-chlorophenol and azo dye remazol red in diffuse indoor daylight conditions (Sakthivel and Kisch, 2003). Ren and coworkers successfully designed a visible light responsive carbon doped titania photocatalyst at low temperature from glucose molecules. The carbon-titania combination produced advanced photocatalytic results than undoped and commercially available Degussa P25 titania photocatalyst for the devastation of RhB dye under visible light (Ren et al., 2007). Incorporation of carbon into  $\text{TiO}_2$  framework results some highly motivated and promising features which are helpful for the harnessing of visible light.

Considering these highly beneficial aspects of carbon doping, it is therefore recommended to apply a different strategy and new material for the development of highly active carbon material which can be utilized in development of new photocatalysts. This motivated us to explore the unique combination of activated carbon (carbon derived from date seeds) with  $\text{TiO}_2$  in designing photocatalysts to further find the possibilities to increase the photocatalytic skills of  $\text{TiO}_2$ . As per literature survey, it is very hard to find any report regarding the synthesis and utilization of novel nanocomposite involving different wt % of activated carbon (AC) derived from date seeds and  $\text{TiO}_2$  as a photocatalyst. It is pertinent to mention here that activated carbon (AC) involved in composite designing was derived from date seeds (as dates are abundantly available in Kingdom of Saudi Arabia). AC could play dual roles of capable electron-acceptor and a photosensitizer to improve the photocatalytic performance of newly designed photocatalyst. Herein, we report the fabrication of novel nanocomposite involving different wt % (5, 10, 25 and 50) of biomass derived activated carbon (AC) and  $\text{TiO}_2$  for the first time and utilized these combination for the photocatalytic reduction of Cr(VI) to Cr(III) and also for the devastation of methylene blue (MB) dye under visible source of light.

## 2. Experimental

### 2.1. Materials

The block copolymer Pluronic F-127 surfactant EO<sub>106</sub>-PO<sub>70</sub>EO<sub>106</sub> (EO = -CH<sub>2</sub>CH<sub>2</sub>O-, PO = -CH<sub>2</sub>(CH<sub>3</sub>)CHO-), molecular weight :12,600 g/mol, TBOT : Ti(OC(CH<sub>3</sub>)<sub>3</sub>)<sub>4</sub>, acetic acid, hydrochloric acid, methanol and ethanol were obtained from Sigma-Aldrich and utilized as it is without any further processing.

### 2.2. Synthesis of mesoporous TiO<sub>2</sub> (m-TiO<sub>2</sub>)

Mesoporous TiO<sub>2</sub> was successfully obtained by sol-gel technique. Briefly, fixed molar ratio of each involved species i.e. TiO<sub>2</sub>/F127/C<sub>2</sub>H<sub>5</sub>OH/HCl/CH<sub>3</sub>COOH (1:0.02:50:2.25:3.75) was taken in the starting solution. Typically, 1.6 g Pluronic F127, 2.3 mL CH<sub>3</sub>COOH and 0.74 mL HCl were homogeneously mixed in 30 mL of ethanol for 30 min and then mixed with 3.5 mL TBOT by dropwise addition (Ismail et al., 2010). The obtained mixture was strongly stirred for 60 min and then put into a Petri dish. Evaporation of Ethanol at 40 °C in humidity chamber with relative humidity of 40% for 12 h followed by 24 h drying of the prepared sample at 65 °C. The product was calcined for 4 h at 450 °C in air maintaining heating rate to 1 °C/min and a cooling degree of 2 °C/min in order to obtain impurity free m-TiO<sub>2</sub>.

### 2.3. Preparation of activated carbon (AC)

Sufficient amount of date seeds were taken and washed thoroughly with water followed by drying. Dried seeds were then crushed in an electrical grinder and sieved to obtain fine powder, followed by sonication in ethanol for 30 min and then evaporate the ethanol at 50 °C for 24 h. At the final step, the powder was heat-treated to a pyrolysis temperature of 500 °C for 3 h, with a slow heating rate of 10 °C/min under the flow of nitrogen gas.

### 2.4. Preparation of AC/m-TiO<sub>2</sub> nanocomposites

AC/m-TiO<sub>2</sub> comprising of variable weight percentages of biomass derived AC (5.0, 10.0, 25.0 and 50.0) has been fabricated using ultrasonication methodology. Typically, calculated amount of AC as per wt% required for particular combination were added to fixed amount of m-TiO<sub>2</sub> in 100 mL of distilled water which then thoroughly ultra-sonicated for 30 min. The resultant suspensions were filtered and washed 4–5 times with distilled water. Resulting wet material put in an oven for overnight at 65 °C in order to get final dried product.

### 2.5. Material characterization

XRD analysis was accomplished on Bruker diffractometer having Cu Kα<sub>1/2</sub>, λ<sub>α<sub>1</sub></sub> = 154.060 pm, λ<sub>α<sub>2</sub></sub> = 154.439 pm radiation (Model: AXS D4 Endeavour X). Exploration of surface morphological features were achieved on field emission scanning electron microscope (Model: JSM-7600F, Japan) and on Transmission electron microscope (Model: JEOL

JEM-2100F-UHR) having well fitted with Gatan GIF 2001 energy filter with distinctive camera (1 k-CCD) operating at 200 kV to provide EEL spectral trends. All samples also passed through FTIR KBr dispersion mode in the range of 400 to 4000 cm<sup>-1</sup> in order to acquire FTIR spectra on Perkin Elmer FTIR spectrometer. The X-ray photoelectron spectroscopy (XPS) was performed on JEOL, JPS 9200: MgKα spectrometer having excitation radiation source (MgKα, pass energy = 50.0 eV (wide scan) and 30 eV (narrow scan), current = 20 mA, voltage = 10 kV). Fluorescence spectrophotometer (Model: F-7000-Hitachi) was utilized to monitor the photoluminescence (PL) response of each sample at an excitation wavelength 300 nm provided by xenon lamp. A diffuse reflectance has been attained in the range of 200 to 800 nm on UV-Vis spectrophotometer (Lambda 950 model: Perkin Elmer) for all samples. Acquired Kubelka-Munk function [F(R) E]<sup>2</sup> vs. absorbed light energy E, plot was exploited to calculate the band gap energy (E<sub>g</sub>) applying below mentioned equation:

$$F(R)E^2 = \left( \frac{(1-R)^2}{2R} \times hv \right)^2$$

### 2.6. Photocatalytic experiments

The efficiency of all newly prepared photocatalysts of pure TiO<sub>2</sub> and different weight percentages of AC doped TiO<sub>2</sub> (5 to 50 wt%) has been examined by photocatalytic reduction of Cr (VI) to Cr (III) i.e. (potassium dichromate K<sub>2</sub>Cr<sub>2</sub>O<sub>7</sub> solution in water) under visible light irradiation source. All photocatalytic examinations were conducted in a quartz photoreactor (150 mL) purchased from Lelesil systems (India) fitted well on magnetic stirrer. Photo-reactor has been provided with water-circulation to avoid any kind of overheating during treatment process. Proper supply of air has been maintained through the photoreactor aperture. Typically, for each reaction, 0.65 g/l of fabricated photocatalysts was transferred to 100 mL solution of potassium dichromate K<sub>2</sub>Cr<sub>2</sub>O<sub>7</sub> with a concentration 0.1 mM (29.5 ppm) along with 2.5 mM of citric acid acting as a reducing agent. The solution was then put in dark for 30 min to count the adsorption behavior of the photocatalyst. A 250 W visible light source has been utilized for irradiation purpose for each experiment. The initial pH of reaction solution was 3.50 whereas the pH at the end of reaction was found to be 3.58. At least two times centrifugation have been done for each withdrawn sample (5 mL) for appropriate removal of photocatalyst from K<sub>2</sub>Cr<sub>2</sub>O<sub>7</sub> followed by absorbance measurement. UV-Vis absorbance spectra of Cr (VI) were measured at λ = 350 nm to evaluate the efficiency of designed photocatalysts using the below equation:

$$\% \text{ photocatalytic activity} = (1 - C_t)/C_o \times 100$$

Where C<sub>o</sub> denotes the equilibrium concentration and C<sub>t</sub> denotes the concentration at a particular irradiation time t. The photocatalytic reduction of Cr(VI) to Cr(III) was monitored from the concentration of peak appearing at λ = 350 nm at different time intervals (Faisal et al., 2019; Celebi et al., 2017). For every experiment, the rate constant (k) for photocatalytic reduction of Cr (VI) to Cr (III) was obtained utilizing the accomplished primary slope from natural logarithm (ln) of absorbance versus exposure time plot by applying linear regression method i.e., first-order degradation kinetics.

### 2.7. Photo-electrochemical experiments

In order to examine the photo-electrochemical performance of newly designed photocatalyst, working electrodes were fabricated applying the below mentioned methodology. A glassy carbon electrode (GCE) with a surface area  $0.071 \text{ cm}^2$  (diameter = 3.0 mm) (BAS Inc., Japan) concealed with a Teflon jacket was successively polished with  $1.0 \mu\text{m}$  diamond paste and  $0.05 \mu\text{m}$  alumina slurry, respectively. The sonicated shiny electrode surface was thoroughly washed with distilled water and ethanol, and finally dried in air. In order to modify the washed electrode, 10 mg of synthesized material was consistently mixed in  $900 \mu\text{L}$  isopropanol and  $100 \mu\text{L}$  Nafion. The as prepared suspension was then sonicated at ambient conditions for one hour, followed by vortex ca. 20 min in order to acquire uniform suspension. Out of this suspension,  $4 \mu\text{L}$  was carefully employed in the form of uniform layered to the previously washed GC electrode and finally dried in an oven for 30 min at  $60 \text{ }^\circ\text{C}$  to attain an active catalytic layer. The electrochemical analysis was carried out on three electrode-based electrochemical workstation (Zahner Zennium, Germany). Ag/AgCl electrode saturated with KCl was taken as a reference while a Pt wire as a counter electrode. For each experiments,  $0.1 \text{ M Na}_2\text{SO}_4$  solution was utilized as an electrolyte. The EIS Nyquist plots were taken at  $0.0 \text{ V}$  applied potential and  $10 \text{ mV}$  signal amplitude, frequency ranging from  $10^{-2}$  to  $10^5 \text{ Hz}$ . A  $400 \text{ W}$  (visible light) GE lamp was utilized as an irradiation source to inspect the photo-responsive performance of the modified electrodes.

## 3. Results and discussion

### 3.1. Structural investigation of AC/m-TiO<sub>2</sub> nanocomposites

Fig. 1 presented the XRD patterns of AC, m-TiO<sub>2</sub> and AC/m-TiO<sub>2</sub> nanocomposites with variable AC wt%. The pattern obtained for AC undoubtedly demonstrates its appearance in amorphous state. Obtained diffraction pattern for undoped TiO<sub>2</sub> confirms the anatase form of TiO<sub>2</sub> with peaks signifying the (101), (004), (200), (211) and (213) lattice

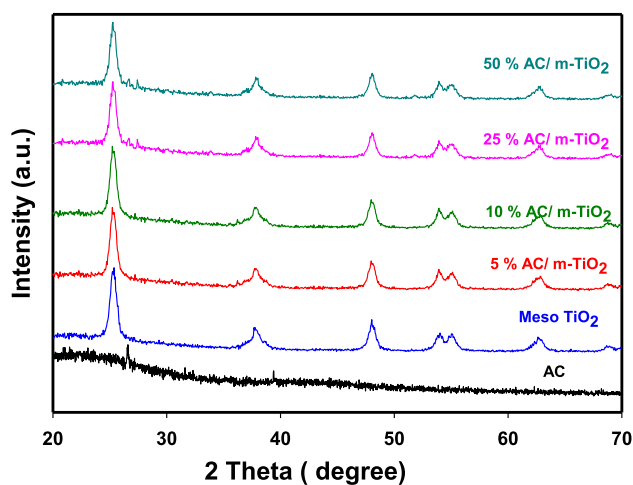


Fig. 1 XRD patterns of AC, m-TiO<sub>2</sub> and AC /m-TiO<sub>2</sub> nanocomposites with variable AC wt%. (5.0–50.0%).

planes suggesting that the titania phase nucleates during the course of heating and subsequently changes into nanocrystals upon calcination at  $450 \text{ }^\circ\text{C}$  (Faisal et al., 2014; Faisal et al., 2014). The obtained peaks are distinct and sharp with no shift in position suggesting sufficient crystallinity and organized framework of the prepared TiO<sub>2</sub>. We could not observe any secondary peaks related to any other phase in case of pure sample, indicating that formed TiO<sub>2</sub> has anatase phase only. As can be seen, after incorporation of AC into TiO<sub>2</sub>, the intensity of main peak (101) at  $2\theta = 43.3^\circ$  for all composite samples remains similar suggesting that the crystallinity of TiO<sub>2</sub> anatase phase remains preserved for all doped frameworks and doping of AC has no notable influence on the lattice organization of TiO<sub>2</sub>. Additionally, the diffraction pattern showed no peak corroborating to AC in all AC/m-TiO<sub>2</sub> framework proposing that AC is either fully disseminated in bulk phase of m-TiO<sub>2</sub> or it is in an amorphous state. A slight lowering in peak intensity in case of 50% AC/m-TiO<sub>2</sub> has been observed which might be due to the formation of hybrid structure.

The functional groups of pure as well as doped samples were determined by Fourier transform infrared spectroscopy (FTIR) as shown in Fig. 2. In case of pure TiO<sub>2</sub>, a broad peak appeared in the range of  $600\text{--}750 \text{ cm}^{-1}$  represents a typical vibration mode of titania (Faisal et al., 2018; Han et al., 2017). FTIR spectrum of biomass derived AC exhibits a highly distinctive absorption peak at  $1610 \text{ cm}^{-1}$  suggesting stretching vibration mode of C = C bond whereas the absorption band at  $1115 \text{ cm}^{-1}$  signifies the stretching vibration mode of C–O linkage (Zhang et al., 2018). The FTIR spectral pattern of all AC doped m-TiO<sub>2</sub> nanocomposites possessed the characteristic absorption peak of AC appearing at  $1610 \text{ cm}^{-1}$  confirming the successful creation of AC/m-TiO<sub>2</sub> which marked the presence of AC in every nanocomposite sample. Furthermore, a small nudge at  $1115 \text{ cm}^{-1}$  is also present in samples of higher concentration of AC (i.e. 25 or 50 wt%) confirming the success of AC/m-TiO<sub>2</sub> formation. As also revealed, the AC efficiently intermingled and created networking with m-TiO<sub>2</sub> with slight shifting which could be ascribed due to weak van der Waals pull between the AC and m-TiO<sub>2</sub> channels (Shahabuddin et al., 2016).

In order to explore the morphology, TEM investigation has been performed for pure TiO<sub>2</sub> and 10% AC/TiO<sub>2</sub> nanocom-

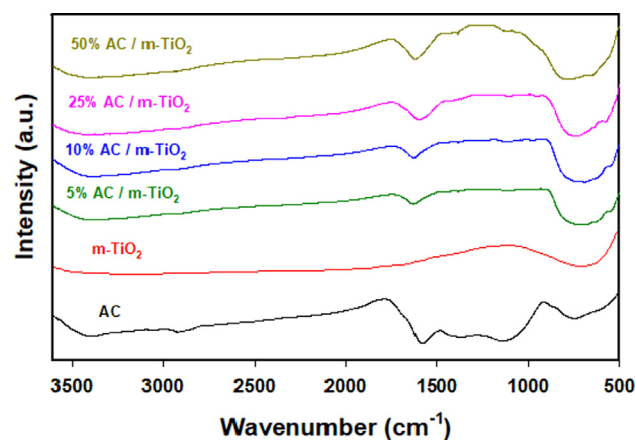
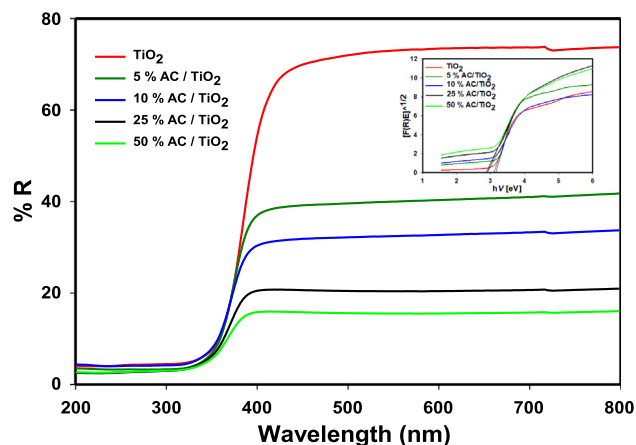


Fig. 2 FTIR spectra measured for AC, m-TiO<sub>2</sub> and AC /m-TiO<sub>2</sub> nanocomposites with variable AC wt%. (5.0–50.0%).

posites as shown in Fig. 3. The TEM analysis of pure TiO<sub>2</sub> shown in Fig. 3 (a) illustrated that pure TiO<sub>2</sub> comprises of almost regular shape nanoparticles grown in high density having little agglomeration. The size of these organized nanoparticles ranges from 8 to 20 nm. Fig. 3 (b), image of 10% AC/m-TiO<sub>2</sub> sample, demonstrates the successful creation of nanocomposite between AC and m-TiO<sub>2</sub>. Obtained image is self-explanatory revealing that m-TiO<sub>2</sub> nanoparticles are in firm coordination or under the blanket of biomass derived AC nanosheets. High resolution TEM analysis of pure TiO<sub>2</sub> is shown in Fig. 3 (c), which exhibited the d spacing or the distance between two adjacent planes is about 0.15 nm which is in agreement with the (211) plane of anatase phase of TiO<sub>2</sub> (Yadav and Sinha, 2017). Fig. 3 (d) exhibits the SAED of 10% AC/m-TiO<sub>2</sub> nanocomposite. Obtained SAED image of the composite reflects highly ordered hollow centric rings signifying the decidedly crystalline characteristic of 10% AC/m-TiO<sub>2</sub> nanocomposite.

All newly created nanocomposites were also examined through diffuse reflectance UV-Vis spectroscopic analysis in order to explore the various optical features of the synthesized materials. The obtained trends are shown in Fig. 4. The well-known fact and observation from UV-Vis spectroscopic analysis is that the optical properties of photocatalyst are correlated to its optical bandgap ( $E_g$ ) energy. For that reason, the Kubelka-Munk (K-M) function  $F(R)$  was determined and plotted to acquire the band gap energy values of different nanocomposites by dropping the tangent lines on Kubelka-Munk (K-M) function vs photon energy curve. Fig. 4 (inset) exhibits the plot following the Kubelka-Munk vs. energy (light) absorbed for 10% AC/m-TiO<sub>2</sub> for the evaluation of band gap. The  $E_g$  for m-TiO<sub>2</sub> is 3.14 eV, perfectly matches with



**Fig. 4** UV-visible diffuse reflectance spectra of for pure m-TiO<sub>2</sub> and AC /m-TiO<sub>2</sub> nanocomposites with variable AC wt%. (5.0–50.0%) and the plots of transferred Kubelka–Munk vs. energy of light absorbed for m-TiO<sub>2</sub> and AC /m-TiO<sub>2</sub> nanocomposites with variable AC wt%. (5.0–50.0%) photocatalysts (Inset).

an earlier report (Faisal et al., 2018). Additionally, the values attained for different nanocomposites with 5, 10, 25 and 50 wt% of AC are estimated to be 3.1, 2.89, 2.88, and 2.88 eV, respectively. Almost all hybrid nanostructures showed lowering in band gap i.e. displaying band gap in the visible region of absorption spectra. The lowering of band gap or absorption in visible region could be highly beneficial during the course of reaction when photo-induced charge transfer occurs.

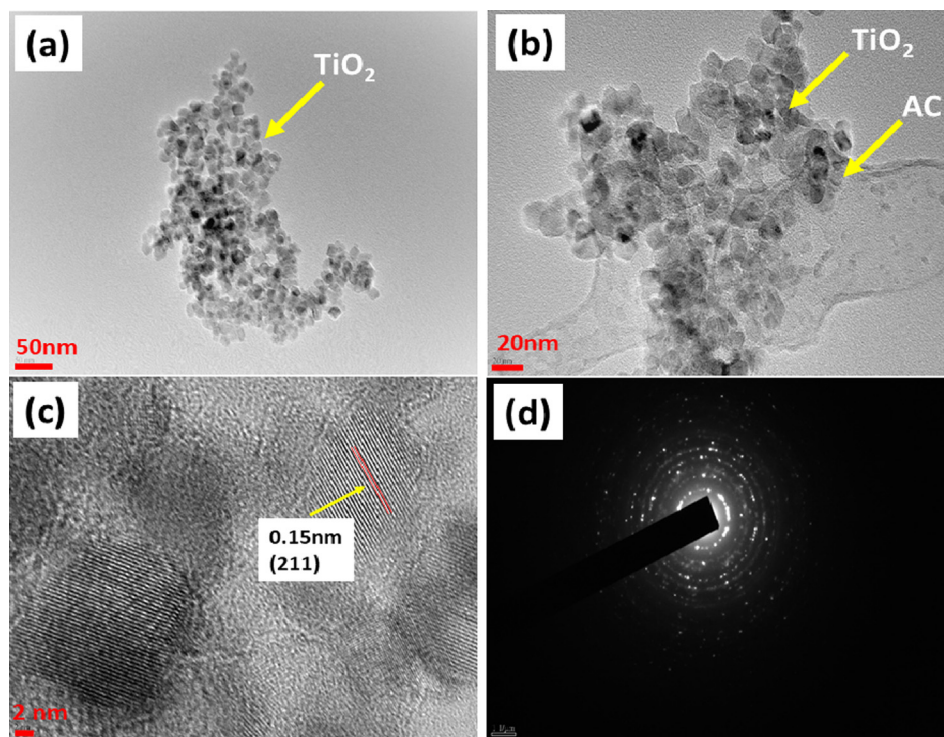


**Fig. 3** TEM images of (a) bare m-TiO<sub>2</sub> (b) 10% AC /m-TiO<sub>2</sub> (c) Higher magnification TEM of pure m-TiO<sub>2</sub> and (d) Selected area electron diffraction of 10% AC /m-TiO<sub>2</sub> photocatalysts.

XPS analysis was performed in order to acquire the surface oxidation states of AC doped m-TiO<sub>2</sub> nanocomposites. Fig. 5 (a) presents the wide scan XPS spectra of 10 %AC/m-TiO<sub>2</sub> photocatalyst, confirming the presence of Ti, C and O elements at their respective binding energy values. Fig. 5 (b) displays the high resolution XPS spectrum of the Ti2p showing two prominent peaks at 458.60 and 464.20 eV which can be assigned to Ti2p doublets, i.e. Ti 2p<sub>3/2</sub> and Ti 2p<sub>1/2</sub>, corresponding to Ti<sup>4+</sup>, confirming the main valence state of + 4 for Ti in AC doped m-TiO<sub>2</sub> (Jia et al., 2018; Xie et al., 2018). Fig. 5 (c) demonstrates the spectrum of C1s with spectral peak at 284.43 eV which represents carbon atom in C-C/C-H moieties (Sivaranjini et al., 2018). Other three deconvoluted spectral peaks centered at 286.19, 288.4 and 292.10 eV signifying the presence of carbon atoms in C-O-C, C = O and O-C = O arrangements (Sivaranjini et al., 2018; Jayaraman et al., 2014). XPS spectrum of oxygen O1s is shown in Fig. 5 (d) where two deconvoluted peaks appeared at binding energy values 529.80 eV and 531.44 eV. The peak marked its presence at 529.80 eV can be ascribed due to the presence of O<sup>2-</sup> ion in

lattice region whereas the peak appeared at 531.40 eV is accredited to O<sup>2-</sup> ion present in oxygen deficient areas (Lee et al., 2012).

The textural properties were further measured for both TiO<sub>2</sub> and AC doped TiO<sub>2</sub> nanocomposite using N<sub>2</sub> adsorption-desorption isotherm as displayed in Fig. 6. As could be revealed, the undoped and the AC doped TiO<sub>2</sub> samples exhibited a typical type IV isotherm with hysteresis profiles observed at higher P/P<sub>0</sub> range, suggesting the formation of mesoporous materials with larger pore sizes. The calculated BET surface area values for both samples are respectively 112.33 and 92.07 m<sup>2</sup>/g for undoped and AC doped TiO<sub>2</sub>. The decrease in BET value for the AC doped TiO<sub>2</sub> sample is likely due to the presence of the AC which might block the access of N<sub>2</sub> molecules into the original structure of the TiO<sub>2</sub>. The total pore volume for the undoped TiO<sub>2</sub> was 0.357504 cc/g while the value obtained for the AC doped TiO<sub>2</sub> was 0.200770 cc/g. The pore size distribution curves are shown in the inset of Fig. 6. It can be noticed that the average pore size of 19 nm was detected in case of m-TiO<sub>2</sub>, whereas the mean pore

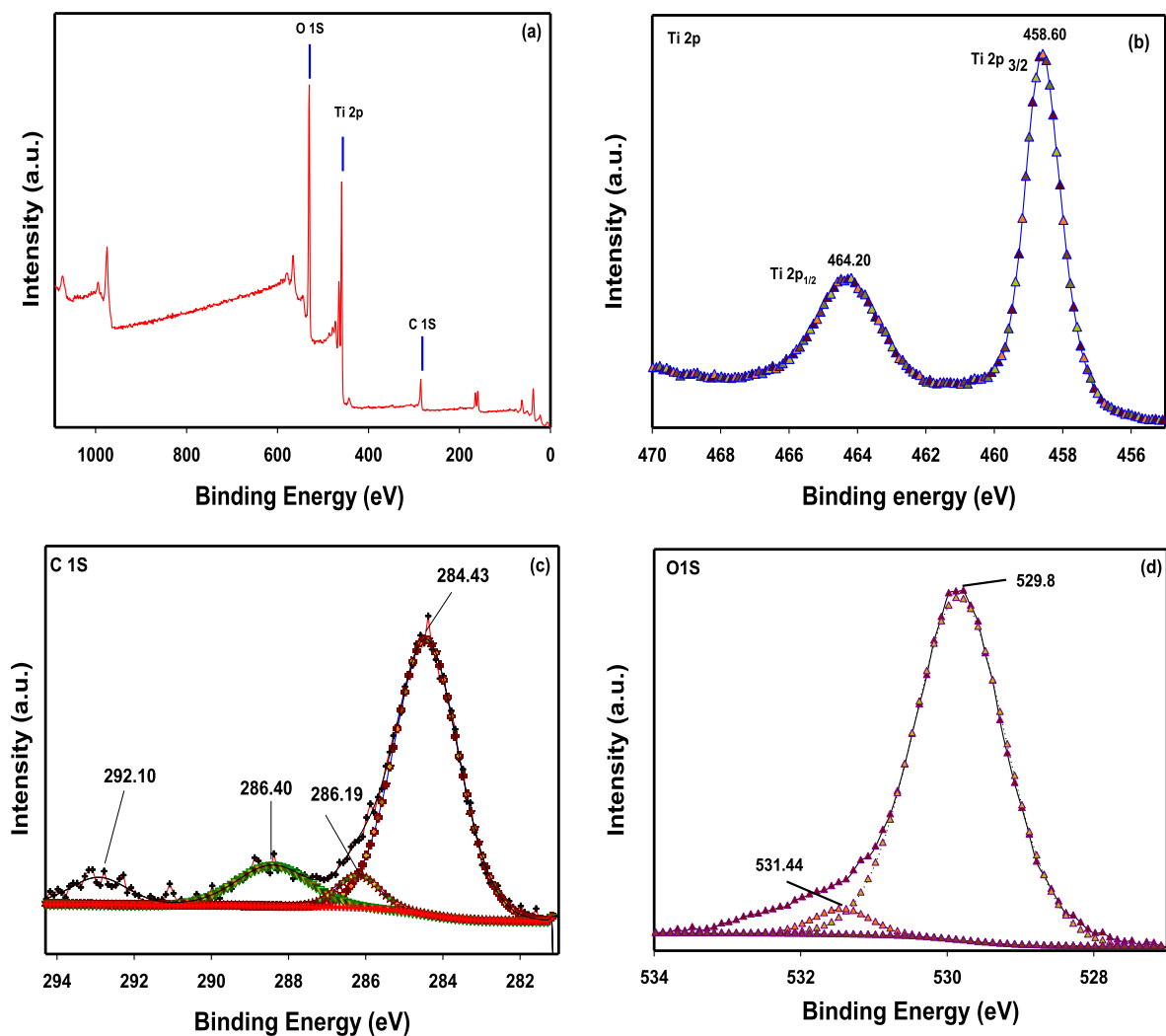


Fig. 5 Wide-scan (survey spectrum) and narrow-high resolution scan XPS spectra of 10% AC /m-TiO<sub>2</sub> nanocomposite photocatalyst. The high resolution scan spectra were recorded for Ti2p C1s and O1s.

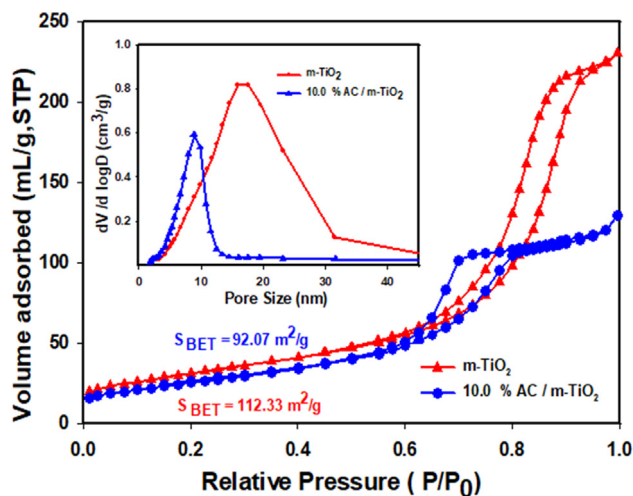


Fig. 6 N<sub>2</sub> sorption isotherm with pore size distribution shown in inset for bare m-TiO<sub>2</sub> and 10% AC/m-TiO<sub>2</sub>.

size of the AC doped m-TiO<sub>2</sub> sample located at the range less than 10 nm, indicating again that the original structure of m-TiO<sub>2</sub> is maintained after the AC doping.

### 3.2. Evaluation of photocatalytic activity

#### Photocatalytic reduction of K<sub>2</sub>Cr<sub>2</sub>O<sub>7</sub>/reduction of Cr (VI) to Cr (III)

All designed nanocomposites have been utilized for the photocatalytic reduction of K<sub>2</sub>Cr<sub>2</sub>O<sub>7</sub> solution under visible light at room temperature. The reduction process can easily be identified by changes taken place in Cr (VI) spectra with irradiation time. The Cr (VI) i.e. K<sub>2</sub>Cr<sub>2</sub>O<sub>7</sub> solution exhibits two distinct peaks marked their presence at ~ 256 and 350 nm (Faisal et al., 2019). The photocatalytic reduction of Cr (VI) was scrutinized by monitoring of the absorption band appearing at 350 nm at regular time intervals. First investigation revealed that when Cr (VI) kept in dark for 30 min, there was no observable reduction of Cr (VI) solution in the presence of newly designed photocatalysts. Also, direct exposure of Cr (VI) solution to visible light source in absence of photocatalysts (blank test) produced no effect or almost negligible percentage of reduction. However, all newly developed nanocomposites i.e. pure m-TiO<sub>2</sub> and different wt% (5.0–50%) of AC doped m-TiO<sub>2</sub> when treated along with 2.5 mmol/L citric acid under visible light source were found to be quite influencing with effective reduction of Cr (VI) solution to various percentages. Amongst various fabricated photocatalysts, the 10% AC/m-TiO<sub>2</sub> was the utmost with highest degree of photocatalytic reduction of Cr (VI) solution and this combination was found to be the most promising among all synthesized products.

Fig. 7(a) collects the results obtained when 10% AC/m-TiO<sub>2</sub> photocatalyst used for Cr (VI) photocatalytic reduction under visible light source. The 10% AC/m-TiO<sub>2</sub> was proven to be highly capable candidate among all, by destructing the prominent absorption band appearing at 350 nm to the ground level with totally flattened after 25 min exposure to visible light irradiation. This highly destructive performance of 10% AC/m-TiO<sub>2</sub> photocatalyst in

just 25 min of exposure to visible light confirmed the potential of this encouraging photocatalytic material.

Fig. 7(b) exhibits the reduction efficiency of various newly synthesized photocatalysts. Achieved results clearly demonstrated that Cr (VI) solution showed no photoreduction tendency when exposed to visible light source in absence of photocatalyst but results were quite encouraging once the solution has been treated in presence of various newly synthesized photocatalysts. Mesoporous titania (m-TiO<sub>2</sub>) was proven to be quite satisfactory, by declining the initial absorption band to 72.0%, i.e. a reduction efficiency ~ 72.0% after 25 min of exposure to visible light irradiation. Under the same testing parameters, the AC doped samples of m-TiO<sub>2</sub> displayed quite elevated performances in comparison to undoped m-TiO<sub>2</sub> towards the accomplishment of reduction process of Cr (VI). Above increment in reduction skills of AC doped samples might be the result of perfect designing of heterojunctions among AC and m-TiO<sub>2</sub>. The outcomes of combined nanostructures are highly motivating and explaining the importance of hetero-structures creation in the field of photocatalysis. Principally, among different newly created AC doped m-TiO<sub>2</sub> hybrid structures, the 10% AC/m-TiO<sub>2</sub> was proven to be supreme candidate with maximum conversion of Cr (VI) target analyte, exhibiting the reduction efficiency of 94.7% in just 25 min irradiation.

The newly designed photocatalysts were additionally scrutinized for the acquisition of highly important parameter i.e. rate constant ( $k$ ) as shown in Fig. 7(c), which directly gives the photodegradation rate value of specific photocatalytic reaction. The rate constant ( $k$ ) increases linearly from  $5.4 \times 10^{-2} \text{ min}^{-1}$ ,  $12.10 \times 10^{-2} \text{ min}^{-1}$  to  $13.15 \times 10^{-2} \text{ min}^{-1}$  as the doping percentage of AC increases from 0 to 10.0 wt % and further increment in AC content (25 to 50 wt%) results in drop in rate constant value. As the AC content increases from 25 to 50 wt%, the active sites of m-TiO<sub>2</sub> were not properly exposed to light source or the active site blockage occurred resulting in lesser production of photogenerated charge carriers i.e. electron and hole pairs and ultimately affected the photocatalytic performance or leading to poor photoreduction by these higher AC content based photocatalysts. The 10% AC/m-TiO<sub>2</sub> sample showed the highest rate constant ( $k$ ) which is ~ 2.44 times higher than that of undoped m-TiO<sub>2</sub>.

Precise band gap engineering or tailoring with flawless synchronization between band gap and formed heterojunctions are highly recommended for the development of novel photocatalytic framework to overcome the problem of recombination process of electron and hole pairs produced during the course of reaction. Rate constant ( $k$ ) values clearly revealed that the 10% AC/m-TiO<sub>2</sub> showed the highest reduction efficiency which might be due to the effective reduction in band gap. Reduction in band gap led to easier and frequent generation of electron and hole pairs under visible light with significant increase in visible light-harvesting, ultimately enhances the performance of designed photocatalyst. Second reason for elevated performance of the 10% AC/m-TiO<sub>2</sub> might be due to the successful creation of heterojunction between AC and m-TiO<sub>2</sub> decidedly key factor in perfect charge separation which in turn led to decline the recombination of photogenerated charge carrier's resulting in extraordinary performance. Our attained photocatalytic reduction trends are in perfect line to our PL analysis. This suggests that the effect of impeccable synchronization between AC and m-TiO<sub>2</sub> offers influential

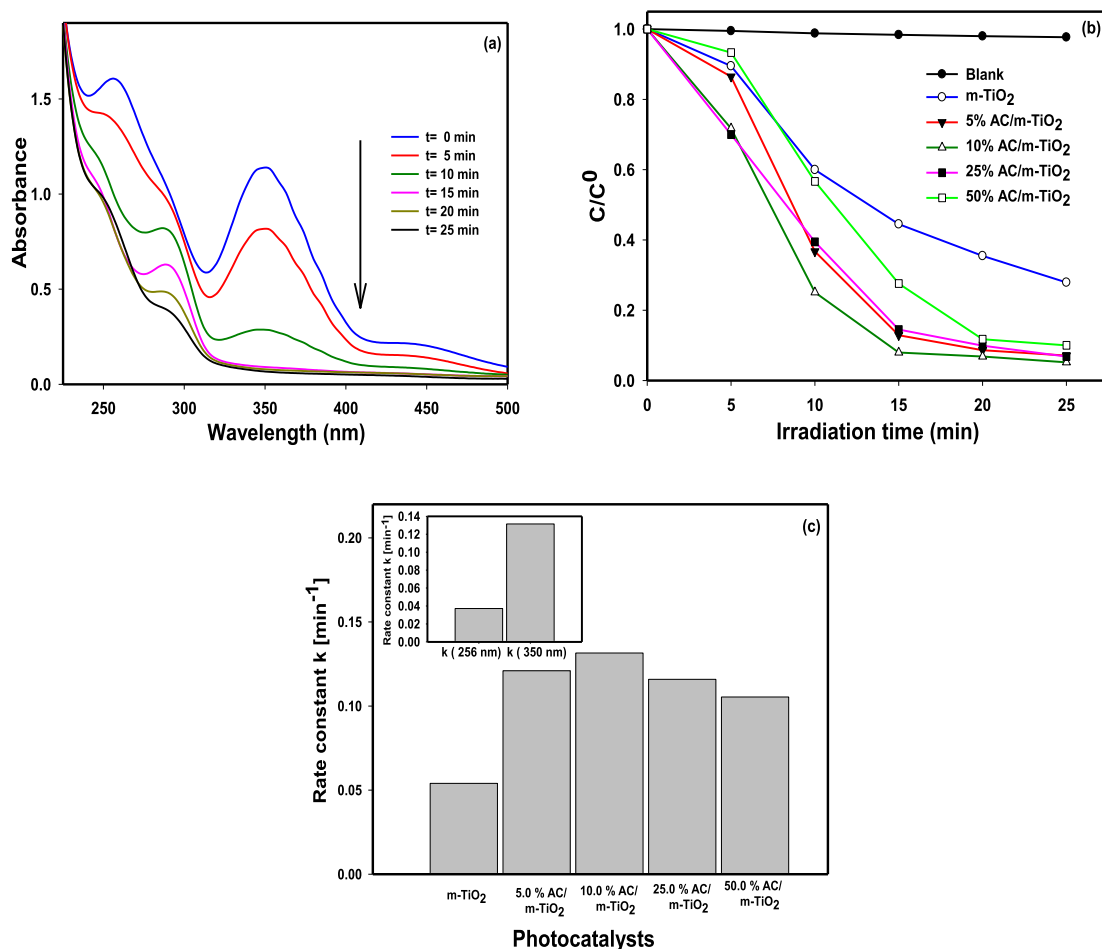


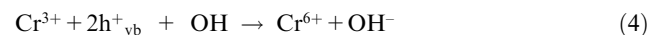
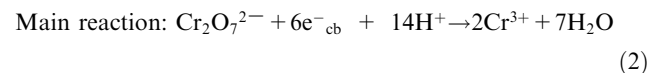
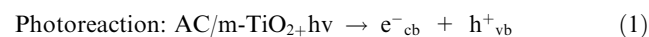
**Fig. 7** (a) Change in the absorption spectra during the photo-reduction of Cr(VI) at different time intervals in presence of 10% AC/m-TiO<sub>2</sub> photocatalysts (b) Change in concentration vs. illumination time of Cr(VI) solution in presence of m-TiO<sub>2</sub> and AC/m-TiO<sub>2</sub> nanocomposites with variable AC wt%. (5.0–50.0%) (c) Comparison of degradation rate for the photo-reduction of Cr (VI).

outstanding performance of the 10% AC/m-TiO<sub>2</sub> towards the conversion of Cr (VI) solution.

It is well recognized that the photocatalytic response of any photocatalyst is markedly dependent on the adsorbing potential of that framework along with superior surficial catalytic skills, significant light harnessing in addition to proficiency in separation of charged species i.e. electrons and holes produced during the process. Mainly, deprived response of separation of photo-generated charge carriers directs faster recombination rate of electrons and holes and is a main drawback that restricts the appropriate functioning of designed photocatalyst. In current investigation, the biomass derived AC nanosheets intermingled with the TiO<sub>2</sub>, as confirmed by FTIR, TEM, EDS and XPS exploration, could provide a sink for electrons produced during the photocatalytic treatment, leading to separation of electrons and holes pairs which in turn boosted the performance of the newly designed material (Hiroshi et al., 2003; Dong et al., 2011). However, the photocatalytic activity using pure TiO<sub>2</sub> as a photocatalyst was low under identical experimental conditions. Significant enhancement in the photo-activity has been displayed by all AC combination with TiO<sub>2</sub> signifying the real value of hybrid structures in photocatalysis. Previous reports have explained that carbon doped TiO<sub>2</sub> possessed sufficient capability and found to be highly

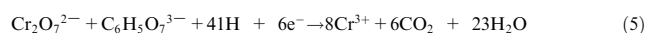
effective in comparison to undoped TiO<sub>2</sub> during the decontamination of aqueous organic pollutants (Hiroshi et al., 2003; Dong et al., 2011). Similarly, in present study, the biomass derived AC led to an effective increment in charge separation efficiency and also directs band gap lowering for extended utilization of visible light.

A probable photocatalytic reduction mechanism of Cr (VI) solution in presence of AC doped TiO<sub>2</sub> under visible light irradiation has been proposed and expressed as follows (Faisal et al., 2019):

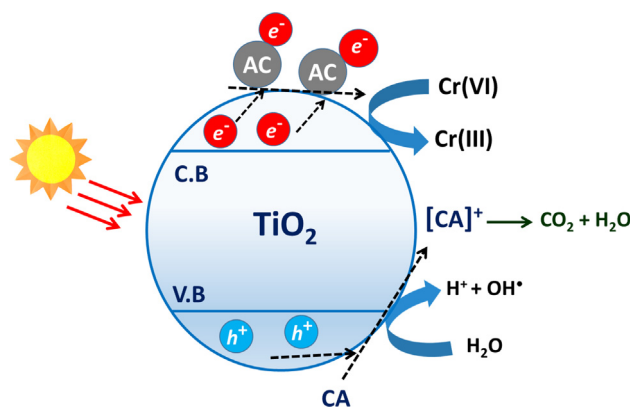


Exposure of AC/TiO<sub>2</sub> nanostructures to visible light irradiation results in generation of e<sup>-</sup> and h<sup>+</sup> pairs with movement of photogenerated electron to conduction band part of designed framework generating hole in valence band. The biomass

derived AC present on the surface of TiO<sub>2</sub> would serve as sink or reservoir for trapping the photogenerated electrons leading to an effective separation of e<sup>-</sup> and h<sup>+</sup>. These electrons readily combined with Cr (VI) to form reduced Cr (III) as shown in Eq. (2). Simultaneously, the photogenerated h<sup>+</sup> in valence band would interact with H<sub>2</sub>O molecules to form highly reactive OH· radicals as shown in Eq. (3). Feasible back interaction of Cr(III) with photogenerated holes and hydroxyl radicals (OH·) radicals could produce Cr(VI) as depicted in Eq. (4). The presence of organic molecule like citric acid (CA) stimulates the photoreduction response of Cr(VI) transformation to Cr(III) in two ways; (a) citric acid efficiently consumed the holes, dropping the chances of back re-oxidation of Cr (III) to Cr(VI) as presented in Eq. (4), and (b) effectively retarded the recombination process of charge carriers by swiftly consuming the photo-generated holes. The above process undoubtedly interpreting that the oxidation of citric acid in presence of light is a sacrificial reaction counteracting the unfavorable re-oxidation process as shown in Eq. (4). Photocatalytic testing carried out in absence of citric acid led to low photo-reduction efficiency for the same photocatalytic conversion process. The minimal citric acid concentration required to attain valuable results was 2.5 mmol/L, below this level of citric acid, separation of e<sup>-</sup> and h<sup>+</sup> pairs was not effective resulting in decline in photo-reduction efficiency. Thus, the whole undergone procedure comprises of photo conversion of Cr(VI) to Cr(III) by exploiting well organized newly fabricated nanostructures under visible light in synchronization with the oxidation of citric acid to CO<sub>2</sub>. The overall pooled reaction can be explained by below Eq. (5) (Yang et al., 2010):



Considering the above discussion, the proposed reduction steps are exemplified in Scheme 1. To further scrutinize the photocatalytic potential or capability of newly designed 10% AC/TiO<sub>2</sub> photocatalyst, it has been further exploited for the demolition of highly organized and stable framework of methylene blue (MB) dye molecule under the same visible light source. Fig. 8(a) displays the demolition trend or decrease in concentration of MB dye by changing in absorption spectra under visible light source. Two highly recognized bands with prominent humps appearing at λ = 291 nm and λ = 663 nm



**Scheme 1** Schematic representation of photocatalytic reduction mechanism of Cr(VI) over AC/TiO<sub>2</sub> photocatalyst; CA = Citric Acid.

very expeditiously shattered in just 25 min in presence of 10% AC/TiO<sub>2</sub> photocatalyst under visible light. Highly encouraging performance by the 10% AC/TiO<sub>2</sub> further clear all ambiguity towards the capability and potential in photocatalytic treatment processes. Previous reports suggested that the flattening of MB structural organization taken place either by (1) oxidative route for the destruction dye molecule or (2) by a two-electron reduction approach transforming the color form of MB to colorless form (leuco-MB) (Zhang and Yu, 2003; Faisal et al., 2020). During the course of whole treatment it was hardly to detect any characteristic peak at λ = 256 nm signifying the leuco-MB, indisputably confirming the removal of MB proceeds via an oxidative approach. The above findings fully support the highly skills of 10% AC/TiO<sub>2</sub> photocatalyst and its bright future in photocatalysis.

The PL examination is a significant approach to get better understanding of photocatalytic excitation mechanism involved. Thus, all newly designed photocatalysts were explored for PL investigation conducted at an excitation wavelength of 300 nm and their respective trends are shown in Fig. 8(b). Obtained PL spectral trends revealed that pure TiO<sub>2</sub> photocatalyst showed the maximum PL intensity while other composite structures with AC showed lower PL intensity spectra. Such lowering in PL spectral intensity denotes an efficient charge separation in case of the composite structures (Ismail et al., 2018; Faisal et al., 2018; Helal et al., 2017). Among all investigated samples, the PL intensity of 10% AC/TiO<sub>2</sub> photocatalyst was found to be the lowest suggesting the highest separation efficiency of charges which directly related to its superior performance. Acquired PL trends are perfectly in accordance with our photocatalytic results.

In any photocatalytic reaction, the role of different active species generated during the course of reaction is extremely important to be examined. Therefore, various trapping experiments have been performed under different scavengers to understand the role played by each active moiety. Typically, for each experiment 0.022 mM of MB dye solution with each scavenger having 0.01 M concentration was taken along with 0.65 g/l of 10% AC/TiO<sub>2</sub> photocatalyst. Hole (h<sup>+</sup>) scavenger i.e. potassium iodide (KI), superoxide radical anions (O<sub>2</sub><sup>•-</sup>) scavenger i.e. ascorbic acid (AA), hydroxyl radical (•OH) trapper isopropyl alcohol (IPA) were utilized during the course of photocatalytic examination (Peng et al., 2017). Obtained results shown in Fig. 9(a) suggested that addition of isopropyl alcohol (IPA) results in the highest retardation in degradation efficiency whereas KI has minimal effect proposing that hydroxyl radicals (•OH) produced the photocatalytic reaction are the main dynamic key players liable for the high level performance of 10% AC/TiO<sub>2</sub> photocatalyst. On the other hand, addition of agents like KI and AA have little or nominal influence, indicating that h<sup>+</sup> and O<sub>2</sub><sup>•-</sup> have supportive role during the treatment of target analyte.

Future prospects and applicability of any newly designed photocatalytic framework fully depend on chief concerning factors which are stability and reproducibility. Therefore, the 10% AC/TiO<sub>2</sub> photocatalyst has been continually exploited for five consecutive photocatalytic reactions for the removal of MB and for the photoreduction of Cr (VI) as shown in Fig. 9 (b) & (c). Obtained results were highly encouraging and motivating where excellent stability with negligible drop in photocatalytic efficiency of 10% AC/TiO<sub>2</sub> photocatalyst. This highly acceptable performance of the newly designed pho-

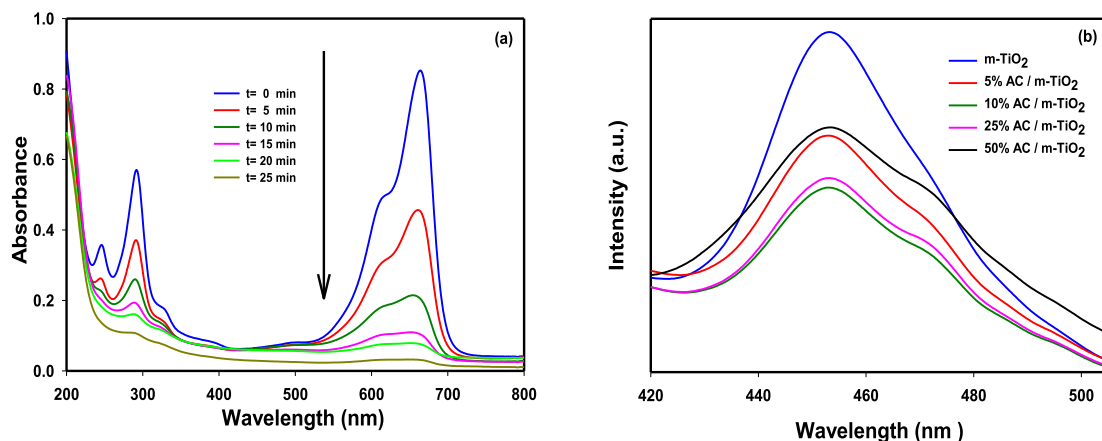


**Fig. 8** (a) Absorbance vs. wavelength as a function of illumination time for the photocatalytic degradation of methylene blue (0.022 mM solution) with 10% AC /m-TiO<sub>2</sub> photocatalysts (b) Room temperature PL spectra at an excitation wavelength 300 pure m-TiO<sub>2</sub> and AC /m-TiO<sub>2</sub> nanocomposites with variable AC wt%. (5.0–50.0%).

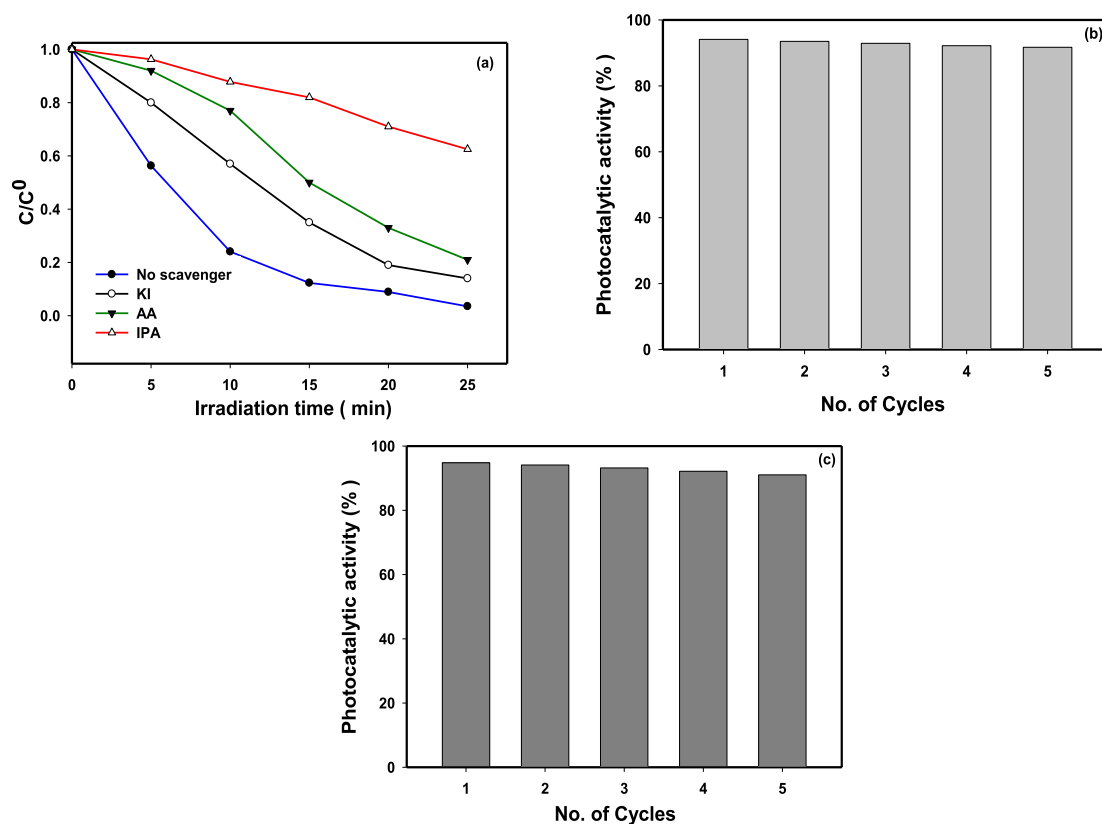


**Fig. 9** (a) Reactive species trapping experiments of the photodegradation of MB under visible light irradiation using 10% AC /m-TiO<sub>2</sub> nanocomposite photocatalyst (b) Repeated cycles up to 5 times of the photocatalytic degradation of MB with 10% AC /m-TiO<sub>2</sub> nanocomposite photocatalyst (c) Repeated cycles up to 5 times of the photo-reduction of Cr(VI) with 10% AC /m-TiO<sub>2</sub> nanocomposite photocatalyst.

photocatalyst opens a new gateway towards its utilization in various environmental concerning issues. Slight drop in photocatalytic efficiency might be due to the loss of photocatalytic material during washing and separation process of photocatalyst for further utilization.

The electrochemically attained impedance spectra (EIS) of bare TiO<sub>2</sub> and 10% AC/TiO<sub>2</sub> nanocomposite layered electrodes were investigated under visible-light source as shown in Fig. 10. The degree or length of the arcs obtained through Nyquist plot is the representative of effectiveness of charge

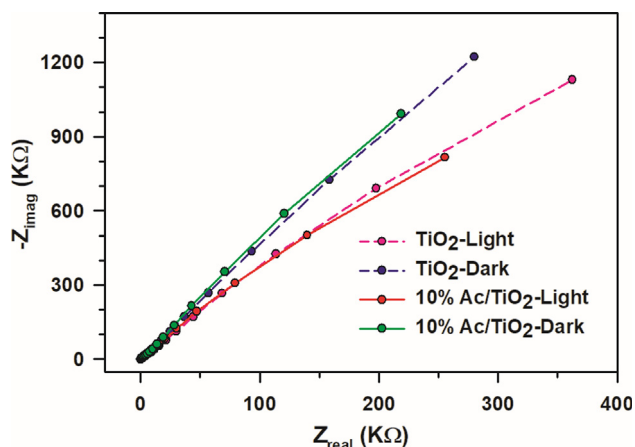


**Fig. 10** EIS Nyquist plots of pure TiO<sub>2</sub> and 10% AC /m-TiO<sub>2</sub> coated glassy carbon electrodes in 0.1 M Na<sub>2</sub>SO<sub>4</sub> aqueous solution at 0.0 V vs. Ag/AgCl (KCl sat.) and 10 mV signal amplitude in the frequency range from 10<sup>-2</sup> to 10<sup>5</sup> Hz with and without light irradiation.

separation or swift movement of electron through the electrode surface. The arc size pattern in obtained plot clearly reveals that bare TiO<sub>2</sub> (dark) arc > bare TiO<sub>2</sub>(light) arc and 10% AC/TiO<sub>2</sub> (dark) arc > 10% AC/TiO<sub>2</sub> (light) arc where 10% AC/TiO<sub>2</sub> nanocomposite under visible-light exposure exhibited the shortest arc, clearly revealing the importance of struc-

tural engineering or modification towards the easier flow of electron and notably decrease in charge transfer resistance. Trends obtained in Nyquist plots unambiguously proven the drop in resistance generated during charge transfer in case of 10% AC/TiO<sub>2</sub> nanocomposite, leading to outstanding results by this newly created photocatalyst. Obtained trends of EIS study are perfect in line to our PL and photocatalytic results.

The EDS results of 10% AC/TiO<sub>2</sub> photocatalyst after the photoreduction analysis are shown in Fig. 11 (a-f). The treated or used photocatalysts i.e. 10% AC/TiO<sub>2</sub> is shown in Fig. 11 (a) whereas Fig. 11 (b) exhibited the very well-developed heterojunction among C, O and Ti. The appearance of chromium in 10% AC/TiO<sub>2</sub> sample after the photoreduction reaction clearly confirmed the adsorbed Cr(III) on AC based TiO<sub>2</sub> photocatalyst. In order to explore the distribution of various components involved in nanocomposites formation, the EDS elemental mapping has also been carried out on reused 10% AC/TiO<sub>2</sub> nanocomposite. The EDS elemental mapping analysis as shown in Fig. 11 (c-f) revealed excellent distribution of C, O and Ti elements, which confirmed the proper homogeneity of the newly designed 10% AC/TiO<sub>2</sub> nanocomposite photocatalyst along with the adsorbed Cr (III) on AC based TiO<sub>2</sub> photocatalyst.

To further confirm the structural recyclability of the current developed photocatalyst, the TEM and HR-TEM images were taken for the 10% AC/TiO<sub>2</sub> nanocomposite photocatalyst after several repeated cycles of the photoreduction of Cr(VI). Fig. 12 (a) and (b) shows the corresponding TEM and

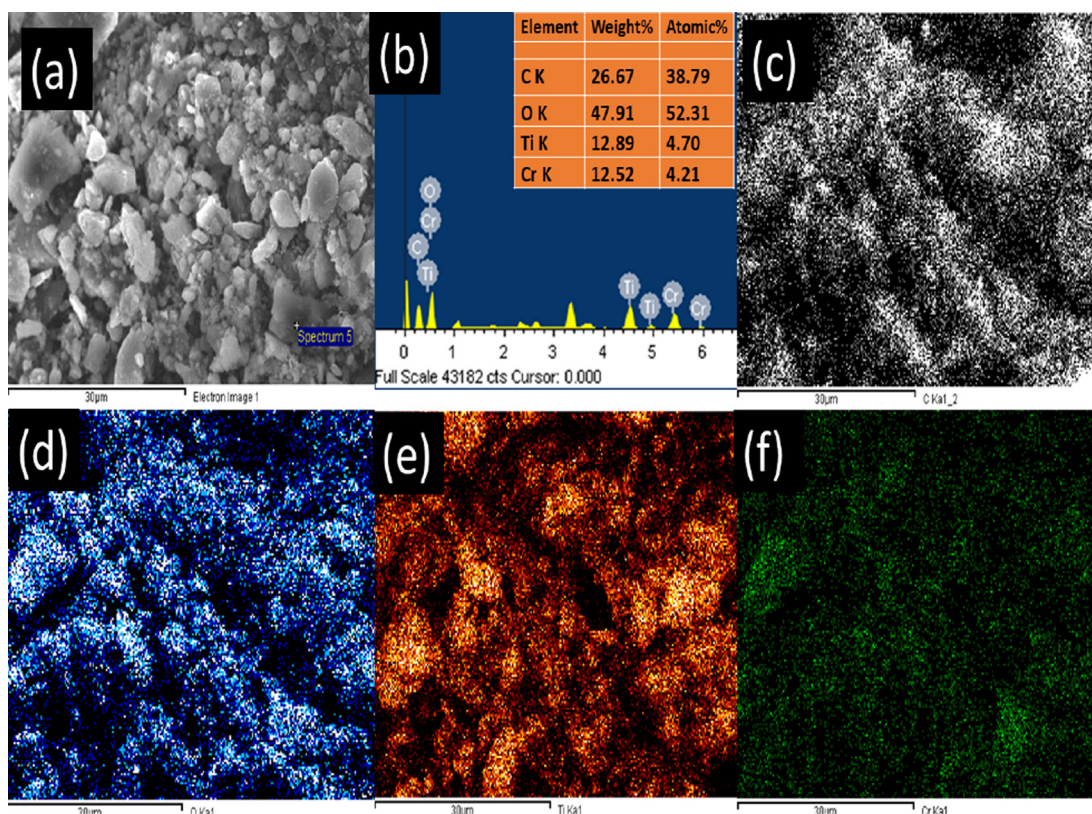


**Fig. 11** After photoreduction process: FESEM images of (a) 10% AC /m-TiO<sub>2</sub> (b) Energy-Dispersive X-ray analysis of 10% AC/m-TiO<sub>2</sub> and EDS elemental mapping (c) C (black) (d) O (blue) (e) Ti (orange) (f) Cr (green) of 10% AC /m-TiO<sub>2</sub> nanocomposite photocatalyst.

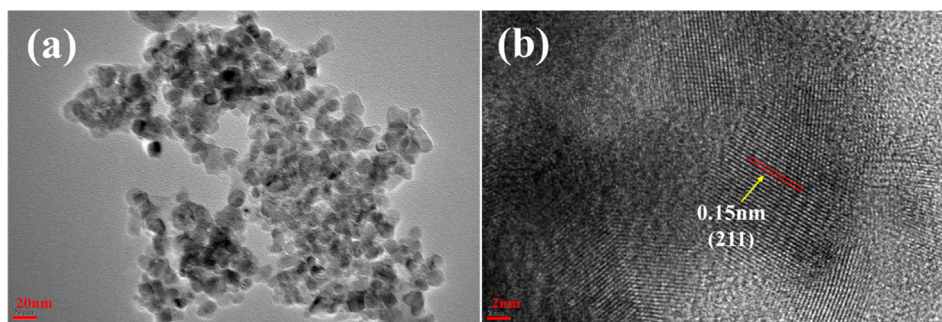


**Fig. 12** After photoreduction process: TEM (a) and HR-TEM (b) images of 10% AC/m-TiO<sub>2</sub> nanocomposite photocatalyst.

HR-TEM images, where one can notice no morphological or structural changes of the reused photocatalyst compared to the original, untreated photocatalyst (please compare TEM images of Fig. 3), confirming the excellent structural recyclability of the 10% AC/TiO<sub>2</sub> nanocomposite photocatalyst.

#### 4. Conclusions

Highly competent visible light driven photocatalysts comprised of various wt % of AC doped TiO<sub>2</sub> have been fabricated by a simple sol-gel approach followed by a sonication technique. Designed AC doped TiO<sub>2</sub> nanostructures were found to be highly impressive and significantly boosted the transformation of Cr(VI) to Cr(III) in presence of citric acid, with photo-reduction efficiency of 94.7% after 25 min, compared to pure TiO<sub>2</sub> which showed a conversion 72.10%. The boosted photocatalytic reduction performance was markedly the result of effectual separation of the photo-generated e<sup>-</sup> and h<sup>+</sup> pairs very well confirmed by the spectral PL analysis. Besides this, the addition of citric acid plays a crucial role by enhancing the conversion process by retarding the unacceptable re-oxidation process of Cr(III) to Cr(VI). Furthermore, the newly designed 10% AC/TiO<sub>2</sub> photocatalyst was found to be highly destructive towards colored species i.e. MB dye when treated under the same visible light conditions. The fabricated photocatalyst exhibited almost same potency after five consecutive cycles with minimum or negligible drop in efficiency and excellent structural recyclability of the photocatalyst.

#### CRedit authorship contribution statement

**Mabkhoot Alsaiani:** Methodology, Investigation, Conceptualization, Formal analysis, Validation, Writing - review & editing.

#### Declaration of Competing Interest

The authors declare that they have no known competing financial interests or personal relationships that could have appeared to influence the work reported in this paper.

#### Acknowledgements

Author is highly thankful to the Deanship of Scientific Research at Najran University, Saudi Arabia for funding this project through a grant research code: NU/ESCI/17/011.

Advanced Materials and Nano-Research Centre, Najran University is highly acknowledged for research facilities.

#### References

- Antonelli, D.M., Ying, J.Y., 1995. Synthesis of hexagonally packed mesoporous TiO<sub>2</sub> by a modified sol-gel method. *Angew. Chem., Int. Ed.* 34, 2014.
- Arpac, E., Sayilkan, F., Asilturk, M., Tatar, P., Kiraz, N., Sayilkan, H., 2007. Photocatalytic performance of Sn-doped and undoped TiO<sub>2</sub> nanostructured thin films under UV and vis-lights. *J. Hazard. Mater.* 140, 69.
- Bouزيد, H., Faisal, M., Harraz, F.A., Al-Sayari, S.A., Ismail, A.A., 2015. Synthesis of mesoporous Ag/ZnO nanocrystals with enhanced photocatalytic activity. *Catal. Today* 252, 20–26.
- Celebi, M., Karakas, K., Ertas, I.E., Kaya, M., Zahmakiran, M., 2017. Palladium nanoparticles decorated graphene oxide: active and reusable nanocatalyst for the catalytic reduction of hexavalent chromium(VI). *ChemistrySelect* 2, 8312–8319.
- Charanpahari, A., Umare, S.S., Gokhale, S.P., Sudarsan, V., Sreedhar, B., Sasikala, R., 2012. Enhanced photocatalytic activity of multi-doped TiO<sub>2</sub> for the degradation of methyl orange. *Appl. Catal. A: Gen.* 443–444, 96.
- Dong, F., Guo, S., Wang, H., Li, X., Wu, Z., 2011. Enhancement of the visible light photocatalytic activity of C-doped TiO<sub>2</sub> nanomaterials prepared by a green synthetic approach. *J. Phys. Chem. C* 115, 13285–13292.
- Faisal, M., Ismail, A.A., Harraz, F.A., Bouزيد, H., Al-Sayari, S.A., Al-Hajry, A., 2014. Highly selective colorimetric detection and preconcentration of Bi(III) ions by dithizone complexes anchored onto mesoporous TiO<sub>2</sub>. *Nanoscale Res. Lett.* 9, Article no 62.
- Faisal, M., Ismail, A.A., Harraz, F.A., Bouزيد, H., Al-Sayari, S.A., 2014. Mesoporous TiO<sub>2</sub> based optical sensor for highly sensitive and selective detection and preconcentration of Bi(III) ions. *Chem. Eng. J.* 243, 509–516.
- Faisal, M., Harraz, F.A., Ismail, A.A., Mohamed El-Toni, A., Al-Sayari, S.A., Al-Hajry, A., Al-Assiri, M.S., 2018. Polythiophene/mesoporous SrTiO<sub>3</sub> nanocomposites with enhanced photocatalytic activity under visible light. *Sep. Purif. Technol.* 190, 33–44.
- Faisal, M., Ismail, A.A., Harraz, F.A., Al-Sayari, S.A., El-Toni, A. M., Al-Salami, A.E., Al-Assiri, M.S., 2018. Fabrication of highly efficient TiO<sub>2</sub>/C<sub>3</sub>N<sub>4</sub> visible light driven photocatalysts with enhanced photocatalytic activity. *J. Mol. Struct.* 1173, 428–438.
- Faisal, M., Harraz, F.A., Ismail, A.A., El-Toni, A.M., Al-Sayari, S.A., Al-Hajry, A., Al-Assiri, M.S., 2018. Novel mesoporous NiO/TiO<sub>2</sub> nanocomposites with enhanced photocatalytic activity under Visible Light illumination. *Ceram. Int.* 44, 7047–7056.
- Faisal, M., Harraz, F.A., Al-Salami, A.E., El-Toni, A.M., Almidy, A. A., Khan, A., Labis, J.P., Al-Sayari, S.A., Al-Assiri, M.S., 2019. Enhanced photocatalytic reduction of Cr(VI) on silver nanoparticles modified mesoporous silicon under visible light. *J. Am. Ceram. Soc.*, 1–11

- Faisal, M., Harraz, F.A., Jalalah, M., Alsaiani, M., Al-Sayari, S.A., Al-Assiri, M.S., 2020. Polythiophene doped ZnO nanostructures synthesized by modified sol-gel and oxidative polymerization for efficient photodegradation of methylene blue and gemifloxacin antibiotic. *Mater. Today Commun.* 24, 101048.
- Faisal, M., Rashed, Md.A., Alhmmami, M.A.M., Harraz, F.A., 2021. Clean light oriented ultrafast Pt/Bi<sub>2</sub>S<sub>3</sub> nanoflakes for the photocatalytic destruction of gemifloxacin mesylate drug and methylene blue. *J. Photochem. Photobiol. A: Chem* 414, 113288.
- Fateh, R., Ismail, A.A., Dillert, R., Bahnemann, D.W., 2011. Highly active crystalline mesoporous TiO<sub>2</sub> films coated onto polycarbonate substrates for self-cleaning applications. *J. Phys. Chem. C* 115, 10405.
- Hahn, R., Schmidt-Stein, F., Salonen, J., Thiemann, S., Song, Y., Kunze, J., Lehto, V., Schmuki, P., 2009. Semimetallic TiO<sub>2</sub> nanotubes. *Angew. Chem., Int. Ed.* 48, 7236.
- Han, C., Shao, Q., Lei, J., Zhu, Y., Ge, S., 2017. Preparation of NiO/TiO<sub>2</sub> p-n heterojunction composites and its photocathodic protection properties for 304 stainless steel under simulated solar light. *J. Alloy. Compd.* 703, 530–537.
- Helal, A., Harraz, F.A., Ismail, A.A., Sami, T.M., Ibrahim, I.A., 2017. Hydrothermal synthesis of novel heterostructured Fe<sub>2</sub>O<sub>3</sub>/Bi<sub>2</sub>S<sub>3</sub> nanorods with enhanced photocatalytic activity under visible light. *Appl. Catal. B Environ.* 213, 18–27.
- Hiroshi, I., Yuka, W., Kazuhito, H., 2003. Carbon-doped anatase TiO<sub>2</sub> powders as a visible-light sensitive photocatalyst. *Chem. Lett.* 32, 772–773.
- Ismail, A.A., Bahnemann, D.W., Robben, L., Yarovyi, V., Wark, M., 2010. Palladium doped porous titania photocatalysts: impact of mesoporous order and crystallinity. *Chem. Mater.* 22, 108–116.
- Ismail, A.A., Bahnemann, D.W., 2010. Metal-free porphyrin-sensitized mesoporous titania films for visible-light indoor air oxidation. *ChemSusChem* 3, 1057–1063.
- Ismail, A.A., Bahnemann, D.W., Al-Sayari, S.A., 2012. Synthesis and photocatalytic properties of nanocrystalline Au, Pd and Pt photodeposited onto mesoporous RuO<sub>2</sub>-TiO<sub>2</sub> nanocomposites. *Appl. Catal. A: General* 431–432, 62–68.
- Ismail, A.A., Faisal, M., Al-Haddad, A., 2018. Mesoporous WO<sub>3</sub>-graphene photocatalyst for photocatalytic degradation of MB dye under visible light illumination. *J. Environ. Sci.* 66, 328–337.
- Ismail, Adel A., Ibrahim Abdelfattah, Faisal, M., Helal, Ahmed, 2018. Efficient photodecomposition of herbicide imazapyr over mesoporous Ga<sub>2</sub>O<sub>3</sub>-TiO<sub>2</sub> nanocomposites. *J. Hazard. Mater.* 342, 519–526.
- Jayaraman, S., Kumar, P.S., Mangalaraj, D., Rajarathnam, D., Ramakrishna, S., Srinivasan, M.P., 2014. Enhanced luminescence and charge separation in polythiophene grafted, gold nanoparticle-decorated, 1-D ZnO nanorods. *RSC Adv.* 4, 11288–11294.
- Jia, T., Fu, F., Yu, D., Cao, J., Sun, G., 2018. Facile synthesis and characterization of N-doped TiO<sub>2</sub>/C nanocomposites with enhanced visible-light photocatalytic performance. *Appl. Surf. Sci.* 430, 438–447.
- Kang, M., 2003. Synthesis of Fe/TiO<sub>2</sub> photocatalyst with nanometer size by solvothermal method and the effect of H<sub>2</sub>O addition on structural stability and photodecomposition. *J. Mol. Catal. A: Chem.* 197, 173.
- Kang, I.C., Zhang, Q.W., Yin, S., Sato, T., Saito, F., 2008. Preparation of a visible sensitive carbon doped TiO<sub>2</sub> photo-catalyst by grinding TiO<sub>2</sub> with ethanol and heating treatment. *F. Appl. Catal., B* 80, 81.
- Lee, C.W., Kim, D.W., Cho, I.S., Park, S., Shin, S.S., Seo, S.W., Hong, K.S., 2012. Simple synthesis and characterization of SrSnO<sub>3</sub> nanoparticles with enhanced photocatalytic activity. *Int. J. Hydrogen Energy* 37, 10557–10563.
- Li, Y., Hwang, D.S., Lee, N.H., Kim, S.J., 2005. Synthesis and characterization of carbon-doped titania as an artificial solar light sensitive photocatalyst. *Chem. Phys. Lett.* 404, 25–9.
- Ly, K., Hua, J., Li, X., Li, M., 2012. Cysteine modified anatase TiO<sub>2</sub> hollow microspheres with enhanced visible-light-driven photocatalytic activity. *J. Mol. Catal. A: Chem.* 356, 78–84.
- Ly, K.L., Zuo, H.S., Sun, J., Deng, K.J., Liu, S.C., Li, X.F., Wang, D. Y., 2009. (Bi, C and N) codoped TiO<sub>2</sub> nanoparticles. *J. Hazard. Mater.* 161, 396–401.
- Mahmoud, M.H.H., Ismail, A.A., Sanad, M.M.S., 2012. Developing a cost-effective synthesis of active iron oxide doped titania photocatalysts loaded with palladium, platinum or silver nanoparticles. *Chem. Eng. J.* 187, 96.
- Muniandy, S.S., Kaus, N.H.M., Z.-Tao Jiang, M. Altarawneh, H.L. Lee, Green synthesis of mesoporous anatase TiO<sub>2</sub> nanoparticles and their photocatalytic activities, *RSC Adv.* 7(2017) 48083.
- Nam, S.-H., Kim, T.K., Boo, J.-H., 2012. Physical property and photo-catalytic activity of sulfur doped TiO<sub>2</sub> catalysts responding to visible light. *Catal. Today* 185, 259–262.
- Niu, B., Wang, X., Wu, K., He, X., Zhang, R., 2018. Mesoporous titanium dioxide: synthesis and applications in photocatalysis. *Energy and Biology, Materials* 11, 1910.
- Ohno, T., Akiyoshi, M., Umebayashi, T., Asai, K., Mitsui, T., Matsumura, M., 2004. Preparation of S-doped TiO<sub>2</sub> photocatalysts and their photocatalytic activities under visible light. *Appl. Catal. A: Gen.* 265, 115.
- Peng, Y., Wang, K.K., Liu, T., Xu, J., Xu, B.G., 2017. Synthesis of one-dimensional Bi<sub>2</sub>O<sub>3</sub>-Bi<sub>2</sub>O<sub>2</sub>.33 heterojunctions with high interface quality for enhanced visible light photocatalysis in degradation of high-concentration phenol and MO dyes. *Appl. Catal. B Environ.* 203, 946–954.
- Petronella, F., Truppi, A., Dell'Edera, M., Agostiano, A., Curri, M.L., Comparelli, R., 2019. Scalable synthesis of mesoporous TiO<sub>2</sub> for environmental photocatalytic applications. *Materials* 12, 1853.
- Ren, W.J., Ai, Z.H., Jia, F.L., Zhang, L.Z., Fan, X.X., Zou, Z.G., 2007. Low temperature preparation and visible light photocatalytic activity of mesoporous carbon-doped crystalline TiO<sub>2</sub>. *Appl. Catal. B* 69, 138.
- Ren, W., Ai, Z., Jia, F., Zhang, L., Fan, X., Zou Z, Z., 2007. Low temperature preparation and visible light photocatalytic activity of mesoporous carbon-doped crystalline TiO<sub>2</sub>. *Appl. Catal. B: Environ.* 69, 138–44.
- Sakthivel, S., Kisch, H., 2003. Daylight photocatalysis by carbon-modified titanium dioxide. *Angew. Chem., Int. Ed.* 42, 4908.
- Sanad, M.M.S., Abdel-Aal, E.A., Osman, H.M., Kandil, A.T., 2018. Photocatalytic reduction of hexavalent chromium with commercial Fe/Ti oxide catalyst under UV and visible light irradiation. *Int. J. Environ. Sci. Technol.* 15, 2459.
- Shahabuddin, S., Sarih, N.M., Mohamad, S., Ching, J.J., 2016. SrTiO<sub>3</sub> nanocube-doped polyaniline nanocomposites with enhanced photocatalytic degradation of methylene blue under visible light. *Polymers* 8, 27.
- Shayegan, Z., C.-Seo Lee, Haghighat, F., 2018. TiO<sub>2</sub> photocatalyst for removal of volatile organic compounds in gas phase – A review, *Chem. Eng. J.* 334, 2408–2439.
- Sivaranjini, B., Mangaiyarkarasi, R., Ganesh, V., Umadevi, S., 2018. Vertical alignment of liquid crystals over a functionalized flexible substrate. *Sci. Rep.* 8, 8891.
- Sonawane, R.S., Kale, B.B., Dongare, M.K., 2004. Preparation and photo-catalytic activity of Fe-TiO<sub>2</sub> thin films prepared by sol-gel dip coating. *Mater. Chem. Phys.* 85, 52.
- Venkatachalam, N., Palanichamy, M., Murugesan, V., 2007. Sol-gel preparation and characterization of alkaline earth metal doped nano TiO<sub>2</sub>: Efficient photocatalytic degradation of 4-chlorophenol. *J. Mol. Catal. A* 273, 177.
- Xiao, Q., Ouyang, L., 2009. Photocatalytic activity and hydroxyl radical formation of carbon-doped TiO<sub>2</sub> nanocrystalline: Effect of calcination temperature. *Chem. Eng. J.* 148, 248.
- Xie, W., Li, R., Qingyu Xu, 2018. Enhanced photocatalytic activity of Se-doped TiO<sub>2</sub> under visible light irradiation. *Sci. Rep.* 8, 8752.

- Yadav, R.K., Sinha, A.K., 2017. Titania cowrapped  $\alpha$ -sulfur composite as a visible light active photocatalyst for hydrogen evolution using in situ methanol from  $\text{CO}_2$  as a sacrificial agent. *ACS Sustainable Chem. Eng.* 5, 6736–6745.
- Yang, L., Xiao, Y., Liu, S., Li, Y., Cai, Q., Luo, S., 2010. Photocatalytic reduction of Cr (VI) on  $\text{WO}_3$  doped long  $\text{TiO}_2$  nanotube arrays in the presence of citric acid. *Appl. Catal. B.* 94, 142.
- Yang, G., Yan, Z., Xiao, T., 2012. Low-temperature solvothermal synthesis of visible-light-responsive S-doped  $\text{TiO}_2$  nanocrystal. *Appl. Surf. Sci.* 258, 4016–4022.
- Zhang, L., Tu, L.-yu, Liang, Y., Chen, Q., Li, Z.-sheng, Li, C.-hai, Wang, Z.-hui, Li, W., 2018. Coconut-based activated carbon fibers for efficient adsorption of various organic dyes. *RSC Adv.* 8, 42280–42291.
- Zhang, W., Tian, Y., He, H., Xu, L., Li, W., Zhao, D., 2020. Recent advances in the synthesis of hierarchically mesoporous  $\text{TiO}_2$  materials for energy and environmental applications. *Natl. Sci. Rev.* 7, 1702.
- Zhang, L.Z., Yu, J.C., 2003. A sonochemical approach to hierarchical porous titania spheres with enhanced photocatalytic activity. *Chem. Commun.* 2078.